Rise and fall of Mott insulating gaps in YNiO₃ paramagnets as a reflection of symmetry breaking and remaking

Oleksandr I. Malyi [*] and Alex Zunger [†]

Renewable and Sustainable Energy Institute, University of Colorado, Boulder, Colorado 80309, USA

The YNiO₃ nickelate is a paradigm d-electron oxide that manifests the intriguing temperature-mediated sequence of three phases transitions from (i) magnetically ordered insulator to (ii) paramagnetic (PM) insulator and then to (iii) PM metal. Such phenomena raised the question of the nature of the association of magnetism and structural symmetry breaking with the appearance in (i) and (ii) and disappearance in (iii) of insulating band gaps. It is demonstrated here that first-principles mean-field–like density-functional theory (DFT), driven by molecular dynamics temperature evolution, can describe not only the origin of the magnetically long-range ordered insulating phase (i), but also the creation of an *insulating paramagnet* (ii) that lacks spin- long-range order, and of a metallic paramagnet (iii) as temperature rises. This approach provides the patterns of structural and magnetic symmetry breaking at different temperatures, in parallel with band gaps obtained when the evolving geometries are used as input to DFT electronic band-structure calculations. This disentangles the complex interplay among spin, charge, and orbital degrees of freedom. Analysis shows that the success in describing the rise and fall of the insulating band gaps along the phase transition sequence is enabled by allowing sufficient flexibility in describing diverse local structural and magnetic motifs as input to DFT. This entails the use of sufficiently large supercells that allow expressing structural disproportionation of octahedra, as well as a description of PM phases as a distribution of local magnetic moments (rather than using a single averaged moment). It appears that the historic dismissal of mean-field–like DFT as being unable to describe such Mott-like transitions was premature, as it was based on consideration of averaged crystallographic unit cells, a description that washes out local symmetry-breaking motifs. The magnetically ordered insulating YNiO₃ phase (i) and the PM insulating phase (ii) result in DFT from allowing symmetry breaking, evident already by considering the athermal internal energy. In contrast, the PM metallic phase (iii) is formed thermally by smearing out thus weakening symmetry breaking. Analysis of snapshots of the different forms of structural vs magnetic symmetry breaking shows that only the loss of the polymorphous distribution of magnetic moments existing in (ii) causes the fall of the band gap, resulting in the metallic state in (iii). The interesting conclusion is that such a description of the rise [in phases (i) and (ii)] and fall [in phase (iii)] of the insulating gap does not rely on the traditional Mott-like strong correlation understanding, but on breaking and remaking of magnetic and structural symmetries reflected in energy lowering.

I. INTRODUCTION

The insulating states both below and above the Néel temperature and the temperature-induced insulator-to-metal transition [1] are characteristic features of many 3d Mott oxide systems [2] that have been considered for neuromorphic computing [3] and transparent conductors [4–7]. From a fundamental perspective, the persistent pertinent questions continue to be (a) understanding the nature of the initial insulating phase that emerges from zero-gap band degeneracy associated with open-shell configuration [8,9]; (b) understanding the nature of the final metallic phase, which depends on whether the final phase is magnetically ordered or not; and (c) understanding the mechanism by which applied "external knobs" (e.g., temperature, pressure, or doping) transform a magnetically ordered insulator (i) or a PM insulator (ii) into a PM metal (iii) [1,2]. Traditionally, the answers were provided within the context of strongly correlated physics where "electron phases" are the key player. The rise of insulating phases (i) and (ii) from a noninteracting zero-gap metal has been conventionally described by electron Coulomb repulsion U (unique to strongly correlated models and absent from mean-field–like methods [10–14]) in a largely unresponsive frozen structure. This gap formation mechanism applies both below the Néel temperature to phases with long-range antiferromagnetic (AFM) order and to higher-T paramagnetic phases that lack long-range magnetic order. The insulating phases (i) and (ii) were traditionally described as large Hubbard U systems, whereas the metallic phase (iii) has been described [14,15] by a weakening of the U/W Coulomb repulsion U with respect to the bandwidth W. Within such "electron phases of matter theories," the microscopic degrees of freedom such as octahedral tilting [16], Jahn-Teller–(like) distortion [17], structural (charge) disproportionation [18–20], and distribution of nonzero local magnetic moments

TABLE I. Summary of the structural, magnetic, and basic electronic properties observed in different $YNiO_3$ phases. DLE denotes double local environment; SLE denotes single local environment , whereas "B" and "M" refer to bond and magnetic motifs.

Phase	Crystal space group	Magnetic order	Electronic properties	Temperature (K)	Structural motif	Magnetic motif
α	$P2_1/n$ (Monoclinic)	AFM	Insulator	$T < 145$ [18,32,33]	B-DLE	M-DLE
β	$P2_1/n$ (Monoclinic)	PM	Insulator	$145 < T < 582$ [18,32,33]	B-DLE	M-DLE
γ	$Pbnm$ (Orthorhombic)	PM	Metal	$T > 582$ K [18]	B-SLE	M-SLE

[8,21–23] are mostly regarded as unresponsive background that is not the cause of the formation of (i)–(iii) but effects that can be considered later. This viewpoint caused an understandable migration of computational efforts that aim to describe phases (i)–(iii) of open-shell d-electron oxides (e.g., $YNiO_3$ [24–28] and $LaTiO_3$ [10,13]) towards strongly correlated methods, leapfrogging mean-field–like methods such as DFT. However, it remains unclear if DFT was thought to fail in this problem because of its inability to describe strong correlation gap formation in the insulating phases (i) and (ii), or because of the lack of proper description of the local motifs in PM phases (ii) and (iii). For instance, it has been recently demonstrated that accounting for energy-lowering formation of distribution of local spin and structural motifs (i.e., using polymorphous description of quantum material) in $3d$ Mott oxides can reproduce insulating nature of the compounds and experimentally observed symmetry breaking without accounting for any dynamic correction [9,21–23,29]. Interestingly, the distribution of local motifs is also observed to be within superposition description [30], Heisenberg Monte Carlo simulation [31], and Landau-Lifshitz-Gilbert spin dynamics [31] of PM phases of quantum materials.

Herein, we focus on $YNiO_3$-one of the most representative cases of rare (R)-earth nickelates $(RNiO_3)$ that contains all the main features that appear in other systems. Its relevant crystallographic and magnetic configuration are summarized in Table I. They consist of two crystal structures (monoclinic and orthorhombic), two magnetic configurations (antiferromagnetic and paramagnetic), and most notably, the existence of either a single repeated motif ["single-local environments" (SLE)] or its disproportionation into two motifs ["double-local environments" (DLE)]. The low-temperature monoclinic α phase exhibits both a bond (B) double-local environment (B-DLE) and magnetic moment (M) double-local environments (M-DLE), meaning it is fully symmetry broken. This monoclinic antiferromagnetic insulator transforms at $T \sim 145$ K to the β phase being a paramagnetic version of the same monoclinic paramagnetic insulator [18,32,33]. At a high temperature of >582 K [18], it further transforms to the γ phase being, as far as is known, the SLE orthorhombic paramagnetic metal.

We show that the key to the present understanding is that whereas strongly correlated philosophy is needed if the paramagnetic phases (ii) and (iii) are described within small and highly symmetric unit cells that exclude symmetry breaking, relaxing this constrain naturally allows energy-lowering symmetry breaking to come into play. It turns out that DFT (as internal energy minimizer) and DFT molecular dynamics (as free-energy equilibration) explain the rise and fall of insu-

lating gaps in $YNiO_3$ paramagnets as a result of structural (magnetic) disproportionation and remaking as illustrated in Fig. 1. We also demonstrate that two types of symmetry breakings are most critical: increased temperature causes the loss of structural bond disproportionation (B-DLE becomes B-SLE). However, it is only the loss of magnetic moment distribution (M-DLE becomes M-SLE) that causes the fall of the band gap and rise of the metallic state. With these advances, it is now possible to determine the nature of the insulating state, metallic state, and the transitions between them without depending on pure electronic effects such as strong correlation.

II. RESULTS

A. Rise and fall of insulating gaps in $YNiO_3$ as a result of symmetry breaking and remaking

Columns (a), (b), (c), and (d) in Fig. 1 summarize the main symmetry breaking effects in DFT regarding structure, magnetic moments, and electronic density of states:

(a) When structural symmetry breaking (i.e., formation of B-DLE) is ignored, the orthorhombic AFM [Fig. 1(a)] phase is a "false metal" with a single octahedral volume and two opposing magnetic moments.

(b) Allowing in Fig. 1(b) for full bond and magnetic DLE results in substantial energy lowering (from 8.17 to 0.66 meV per atom) and gives an insulator for the PM monoclinic β phase. Notably, there is a clear presence of M- and B-DLE – i.e., half of Ni atoms have average magnetic moments of $\pm 1.25 \mu$ and 0μ with large and small octahedra of distinct volumes. Such symmetry breaking is sufficient to open the gap, as seen in the calculated density of states (DOS) in Fig. 1(b), without the need to involve a dynamic strong correlation.

(c) As Fig. 1(c) indicates, at 200 K (at which the PM β phase exists experimentally), B-DLE is clearly present in *ab initio* molecular dynamics (AIMD), as shown by the district distribution of NiO_6 octahedral volumes. These results are similar to those observed based on internal energy minimization for the PM β phase [Fig. 1(b)] but are broadened, yet preserving the broken symmetry structure. This broadening of local motif distribution is mainly caused by temperature-induced atomic displacements and volume distribution. The broadening of local spin motifs is also reflected in the distribution of magnetic moments, as shown in Fig. 1(c). This distribution is similar to that observed by internal energy minimization with some additional temperature broadening.

(d) As Fig. 1(d) shows, as temperature further increases (e.g., $T = 600$ K, where the PM γ phase exists experimentally), thermal displacements overwhelm the tendencies from internal energy minimization [Fig. 1(b)], leading to a single Gaussian-like distribution of octahedral volumes and
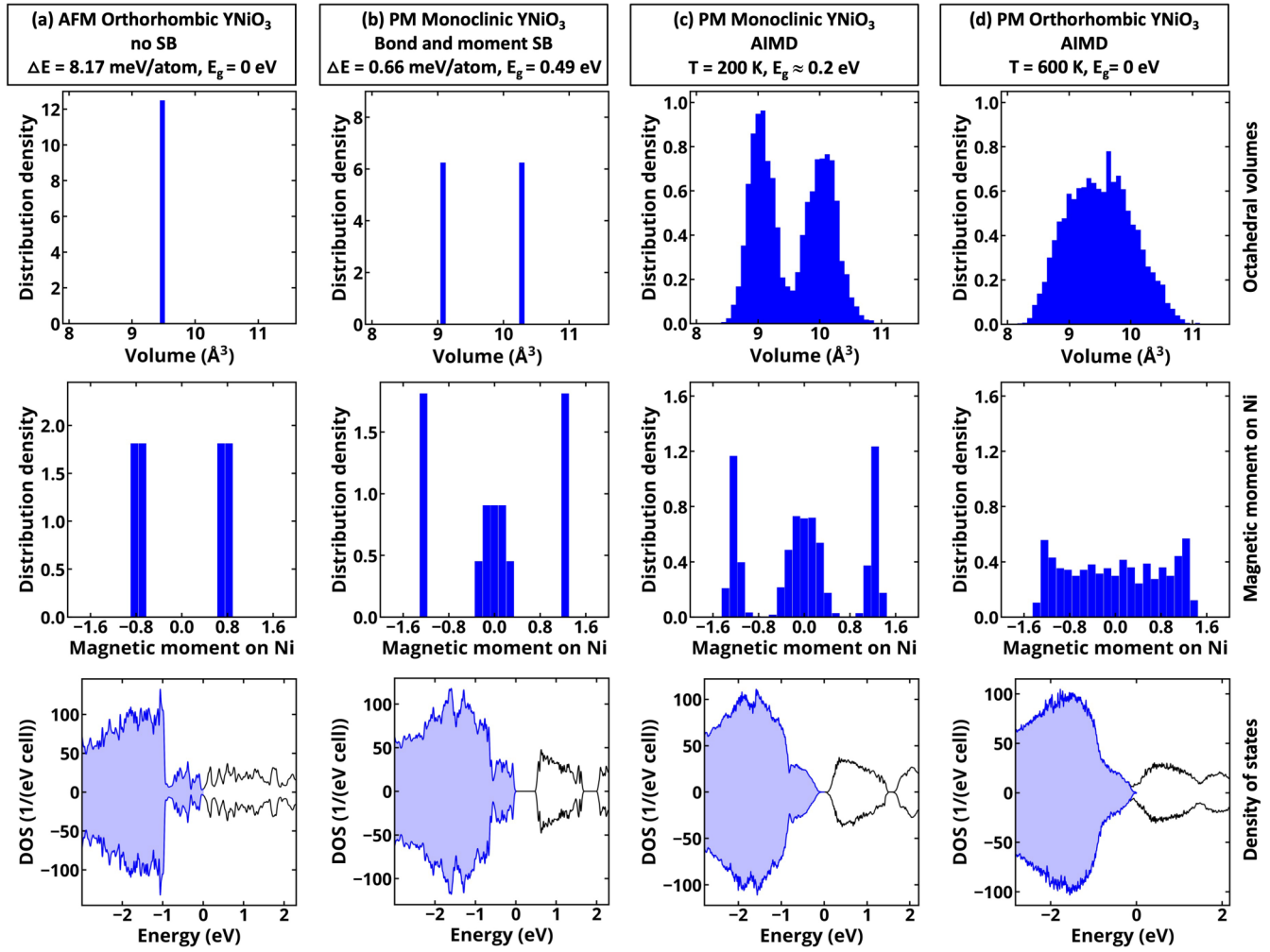
FIG. 1. Octahedral volume (first row), local magnetic moments on Ni sublattice (second row), and electronic density of states (third row) from the first-principles calculations of $YNiO_3$. The four columns describe these results as obtained by a sequence of approximations: Column (a) uses a hypothetical monomorphous structure without symmetry breaking (SB), indicating a single characteristic volume and a simple distribution of local moments leading to a metallic zero band gap. Column (b) uses a spin polymorphous structure obtained by replacing an average monomorphous unit cell with a polymorphous supercell structure. This creates a distribution of different octahedral volumes and a nontrivial distribution of local moments, leading to an insulating gap and a significant stabilization in total energy. Column (c) shows *ab initio* molecular dynamics simulation of spin polymorphous lattice at 200 K, and column (d) shows the same as (c) but at 600 K. Symmetry-broken sharp distribution of different unit-cell volumes and moments seen in column (b) is broadened at 200 K in column (c), reducing the band gap. At the temperature of 600 K [column (d)], thermal displacements overwhelm the tendencies from internal energy minimization, thus completing the insulator to metal transition. Averaged DOS for occupied states are shown as a shadowed region.

disappearance of the two types of magnetic sublattice [Fig. 1(d)]. As one can see at 200 K (under which PM β phase exists), the system is an insulator, while at temperature increase to 600 K (i.e., the lowest temperature at which PM γ phase exists experimentally) the system becomes metal.

The results of Fig. 1 explain, from the point of view of simultaneous electronic vs structural and magnetic response, the role of symmetry breaking in the rise and fall of insulating states. Yet, the roles of individual types of symmetry breaking, such as bond disproportionation (B-SLE becomes B-DLE) or spin disproportionation (M-SLE becomes M-DLE) are not explained. In the next section, we will analyze this by calculating the gaps and energy of individual symmetry-breaking snapshots described in Sec. II B, isolating the critical contributions.

B. Framework for establishing what controls metallization: Loss of structural bond disproportionation or the loss of magnetic moment disproportionation

We will find that increased temperature causes the loss of structural bond disproportionation (B-DLE becomes B-SLE). However, it is only the loss of magnetic moment distribution (M-DLE becomes M-SLE) that causes the fall of the band gap and rise of the metallic state. To demonstrate this physics, we create a "string of steps" (1,2,3, etc.) explained in Fig. 2. We start from high-symmetry orthorhombic $YNiO_3$ structure (B-SLE and M-SLE) and allow one additional type of symmetry breaking or temperature at each step. The simplest case shown in Fig. 2(i) is where the octahedra are all identical in shape and volume, and the magnetic moment is also fixed throughout the crystal. This "bond-SLE" as well as "moment-
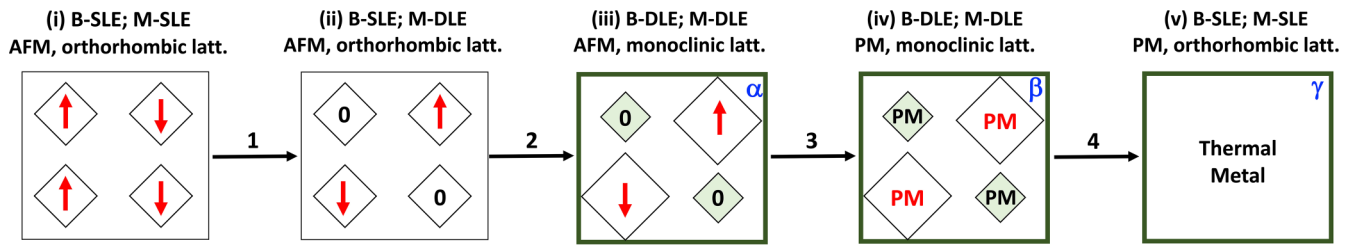
FIG. 2. Schematic illustration of (i-v) different moment (M) and bond (B) environments in $YNiO_3$ and transitions between them used to identify the band-gap opening and metallization. Bold frames denote physical phases from Table I.

SLE" can thus be represented by repeating as a single repeated motif ("monomorphous"). The next step [Fig. 2(ii)] illustrates a unit cell made of a mixed B-SLE with M-DLE, whereas Fig. 2(iii) illustrates the case of a bond-DLE (characterized by two different octahedra, small and large), and moment-DLE (characterized by two different magnetic motifs-zero or finite moment). Different periodic assemblies of bond- and moment-SLE and -DLE motifs make up phases of the crystal realized in crystallographic (monoclinic or orthorhombic) and spin (antiferromagnetic and paramagnetic) configurations. For example, the fully disproportionated unit cell of B-DLE/M-DLE can exist in an AFM monoclinic phase [Fig. 2(iii)], or as a PM monoclinic phase [Fig. 2(iv)], or a PM orthorhombic phase [Fig. 2(v), etc.].

We next describe the first-principles results in the sequence of transformation shown in Fig. 2.

Transformation 1 (Figs. 2 and 3): The monomorphous assumption consisting of a single structural and magnetic motif [B-SLE/M-SLE], predicts a (false) metal [Fig. 1(a)]. However, magnetic disproportionation leads to gapping even without bond disproportionation (Fig. 3).

While the observed α phase of $YNiO_3$ has both bond and magnetic disproportionation (i.e., different-size NiO_6 octahedra and magnetic moments on Ni sublattice) and is an insulator, we wonder if B-DLE is the necessary factor needed to open the gap in $YNiO_3$ relative to the monomorphous state. To answer this question, we have explored the electronic properties of orthorhombic $YNiO_3$ with frozen B-SLE structure, allowing different types of AFM spin configurations. The M-SLE spin configuration has each Ni atom with the same magnetic moments (0.76μ). Since, in this M-SLE, all octahedra have the same spin environment, band-gap opening cannot occur. This, however, does not necessarily mean that band-gap opening requires bond disproportionation. As shown in Fig. 3, we identify an M-DLE configuration as an insulator with a band gap of 0.26 eV. In such an M-DLE spin configuration, half of the Ni atoms have magnetic moments of 1.06μ while the other half has zero magnetic moments, demonstrating that magnetic disproportionation can open the gap even if there is no bond disproportionation.

Transformation 2 (Figs. 2 and 4): Bond disproportionation B-DLE under constant M-DLE enhances the magnitude of the
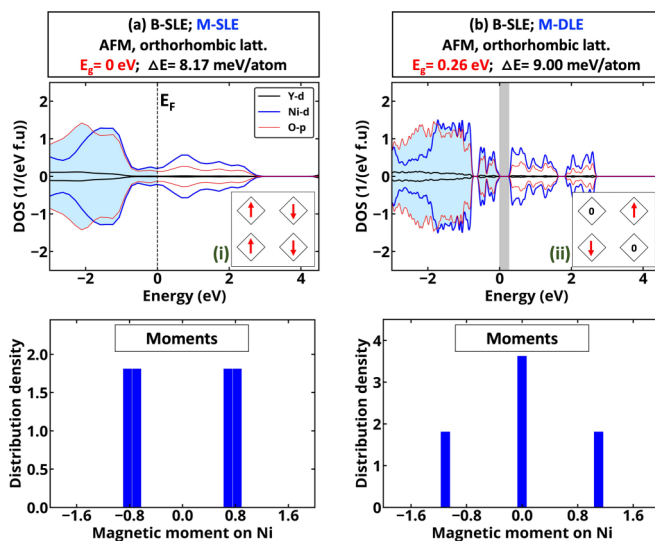

FIG. 3. Magnetic disproportionation (transition 1) can be the cause of gapping even if there is no bond disproportionation present (i.e., all octahedra are equal). (a) B-SLE/M-SLE monomorphous phase consisting of a single structural and magnetic motif predicts a (false) metal, but (b) magnetic disproportionation alone leads to gapping even without bond disproportionation. Relative energy (ΔE) of different phases is given with respect to AFM α phase.
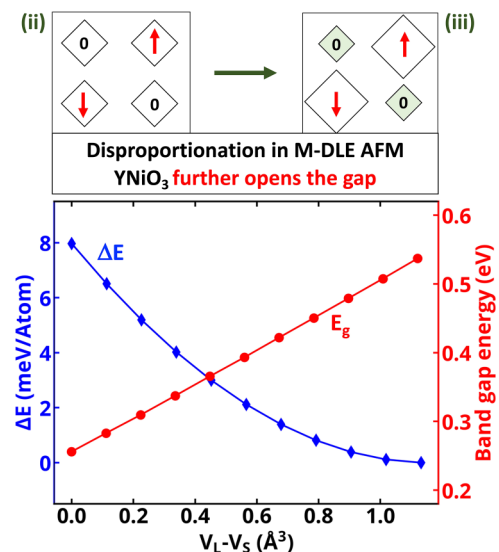

FIG. 4. Bond disproportionation under constant M-DLE (transition 2) enhances the magnitude of the gap created by magnetic disproportionation. Relative internal energy and band-gap energy of AFM M-DLE $YNiO_3$ with orthorhombic lattice vectors as a function of bond disproportionation. Degree of disproportionation is defined as the difference in volumes for large and small NiO_6 octahedra (i.e., 0 volume difference corresponds to SLE orthorhombic structure).
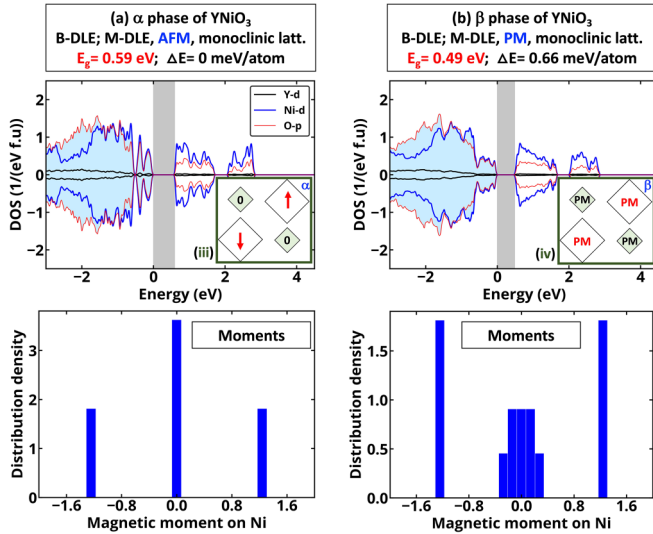
FIG. 5. Néel AFM α to PM β monoclinic transition (transition 3) under constant B-DLE and M-DLE results in the band-gap reduction. Electronic density of states (top figures) and distribution of local magnetic moments on Ni atoms for (a) α- and (b) β phases of $YNiO_3$. For both systems, internal structures and lattice vectors are allowed to relax. Energy difference is given with respect to the α phase (i.e., AFM S-DLE M-DLE monoclinic $YNiO_3$).

band gap created in the first place by magnetic disproportion-ation (Fig. 4).

To understand the role of bond disproportionation on the metal-nonmetal characteristic of $YNiO_3$, we explore the evolution of the band gap as a function of volume difference between large and small octahedra, starting from B-**SLE**/M-DLE transforming into the B-**DLE**/M-DLE α phase. The results are shown in Fig. 4 and demonstrate that octahedral disproportionation is spontaneous, i.e., results in energy lowering. Importantly, the band-gap energy is a linear function of the degree of bond disproportionation and is in-creasing monotonically from 0.26 eV for B-SLE to 0.54 eV for the lowest energy B-DLE structure. Bond disproportiona-tion also affects the magnetic moment on the small octahedra, increasing it from 1.06μ for B-**SLE**/M-DLE, to 1.23μ for B-**DLE**/M-DLE. These results thus further confirm that bond disproportion is only an enhancer of the gapping effect caused in the first place by spin disproportionation. We also note that Alonso *et al.* [18] reported neutron powder-diffraction experi-mental data for the α phase pointing out that the results can be understood as the existence of two Ni sublattices with 1.4 and 0.7μ magnetic moment providing the best fit ($R_{\mathrm{mag}} = 15\%$) for main magnetic reflections. However, the precise measure-ments of magnetic moments and their special distribution require using the magnetic pair-distribution function analysis which was not done in the seminal work of Alonso *et al.* [18] and can further be used to understand spin symmetry breaking in $YNiO_3$ phases.

Transformation 3 (Figs. 2 and 5): The Néel AFM α to PM β transition under constant B-DLE and M-DLE, results in band gap reduction (Fig. 5), but PM β phase is an insulator within mean-field DFT.

For a long time, it has been believed that mean-field theory cannot describe properties of paramagnetic compounds as

such compounds were usually described using global average structure (i.e., *nonmagnetic* model), resulting invariably in a metallic state often conflicting with experimental results. Even in the case of $YNiO_3$, it was argued that DFT cannot do so, indicating, for instance, that "bond-length dispropor-tionation and associated insulating behavior are signatures of a novel correlation effect" [34]. Recently, it has been pointed out [8,21–23,31,35] that band theory can describe param-agnets without appealing for strong correlation by allowing for larger than minimal (super) cells, that permit symmetry breaking and finite local magnetic moments should it lower the total energy. This approach is illustrated here (Fig. 5) for the transition from the α AFM to the β PM phase, in-dicating the formation of a distribution of local Ni magnetic moments in the PM phase. While the α phase has only two magnetically inequivalent sites, in the β phase each Ni has its own magnetic moment, which is due to breaking long-range spin order. Such symmetry breaking results in the band-gap reduction: the band-gap energy for α AFM to β PM phases are 0.59 and 0.49 eV, respectively. These results thus demonstrate that mean-field DFT can accurately represent experimentally observed insulator nature of PM β phase and bond dispropor-tionation despite opposite claims in "correlated" literature.

Transformation 4 (Fig. 2): The PM β insulating phase transforms to a PM γ metallic phase at high temperature due to temperature broadening bond and magnetic disproportion-ation to the point of removing symmetry breaking [Fig. 1(d)].

The explanation of transformation 4 of an *insulating* PM β phase due to the creation of a polymorphous distribution of local moments [8,21,22,35] still faced the need to explain a metallic PM γ phase at higher temperatures (Table I). One might initially suspect that perhaps the PM β phase being insulator, whereas the PM γ phase being metallic might have something to do with the former being monoclinic and the lat-ter being orthorhombic. However, orthorhombic PM structure has a spontaneous tendency towards bond and structural dis-proportionation resulting in band-gap opening. Only at high temperatures [Fig. 1(d)], the internal tendency of the system to energy lowering can be overcome by entropy contribution, which thus eventually results in insulator-metal transition at high temperatures as both bond and magnetic disproportiona-tion are suppressed. We note, however, that even at such high temperatures, the PM γ phase has a distribution of nonzero magnetic moments, and hence the materials properties cannot be described within the nonmagnetic approximation of the paramagnet.

III. DISCUSSION

For a long time, band-structure models of PM phases of oxides have assumed a single structural motif (e.g., octahedron volume) and a single magnetic motif, leading to the monomorphous model representing an effective average configuration. Since such model was nonmagnetic, calcula-tions invariably resulted in a metallic state [36,37]. In the many cases where such predicted metallic phases were in conflict with experimental observations, it was argued that these are, in fact, Mott insulators, so the predicted false-metal character should be resolved by accounting for strong correlation, codified by the on-site Coulomb repulsion U

which splits degenerate bands into occupied and empty. We point out that the existence of a gapped PM phase can be naturally described by mean-field DFT without recourse to a strong correlation. This generally requires that one allows for a larger than a minimal unit cell, enabling structural and/or magnetic symmetry breaking. This leads to a polymorphous structure rather than a virtual averaged structure. Interestingly, $YNiO_3$ has two paramagnetic phases: one at low temperatures being a gapped insulator (β) and one at the higher temperature being ungapped metal (γ). This poses an interesting conundrum as to how those behaviors existing in the same system can be understood. The interesting answer pointed out here is that a gapped insulating phase is evident in first-principles mean-field band theory already via minimizing the internal energy alone in an extended supercell. This leads to a polymorphous network having a distribution of both structural and magnetic motifs (whose average is the irrelevant monomorphous approximant). The motif distribution of this athermal polymorphous structure is inherited by the β phase observed in finite-temperature AIMD. As the temperature increases, AIMD shows that the distinct local structural and magnetic motifs lose their polymorphous distribution; when such geometries are used in band theory, a gapless metallic PM γ phase emerges. Thus, the metallic PM phase emerges from the insulating PM phase not necessarily because of loss of electron correlation but because of thermal motion-induced displacements that alter the electronic band structure.

ACKNOWLEDGMENTS

APPENDIX: DFT DETAILS

The first-principles calculations are carried out using plane-wave DFT $+ U$ as implemented in the Vienna *Ab initio* Simulation Package (VASP) [38–40] with PBEsol (Perdew-Burke-Ernzerhof (PBE) functional revised for solids) [41]. For all calculations, a rotationally invariant approach introduced by Dudarev *et al.* [42] with $U - J$ values of $U = 2$ eV and $J = 0$ applied on Ni-d states is utilized. We recall that U in DFT $+ U$ acts primarily to reduce the mean-field self-interaction in DFT, and thus does not have the same role as U in Hubbard model (i.e., strong correlation). The cutoff energies for the plane-wave basis are set to 500 eV for final calculations and 550 eV for volume relaxation. Atomic relaxations are performed until the internal forces are smaller than 0.01 eV/Å unless specified. Analysis of structural properties and visualization of computed results are performed using VESTA [43] and PYMATGEN library [44]. The paramagnetic phase of $YNiO_3$ is simulated by using the *spin* special quasirandom structure [45] by decorating a 160-atom supercell with spin up and spin down to create a global zero-moment configuration closest to the high-temperature limit of a random spin paramagnet [31]. AIMD simulations are done using the *NPT* ensemble with an *NPT* thermostat for 30 ps with the time step of 1 fs. For AIMD simulations, the averaged density of states for N snapshots has been calculated from molecular dynamics snapshots as $DOS = \frac{\sum_i^N DOS_i}{N}$, where DOS_i of different snapshots are aligned using O-1s core states. The volume of each octahedron was calculated as the convex hull volume for each octahedron. For each AIMD simulation, 200 snapshots are extracted from molecular dynamics simulations after an equilibration period of 10 ps. The distribution of magnetic moments and density of states are computed by averaging of corresponding quantities for 40 snapshots of *ab initio* molecular dynamics simulations after equilibration for 10 ps. The DOS for different snapshots is aligned using O-1s core states.

[1] M. Imada, A. Fujimori, and Y. Tokura, Metal-insulator transitions, Rev. Mod. Phys. **70**, 1039 (1998).

[2] N. Mott, *Metal-Insulator Transitions* (CRC Press, London, 1990).

[3] P. Schofield, A. Bradicich, R. M. Gurrola, Y. Zhang, T. D. Brown, M. Pharr, P. J. Shamberger, and S. Banerjee, Harnessing the metal—insulator transition of VO_2 in neuromorphic computing, Adv. Mater. 2205294 (2022).

[4] L. Hu, M. L. Zhao, S. Liang, D. P. Song, R. H. Wei, X. W. Tang, W. H. Song, J. M. Dai, G. He, C. J. Zhang, X. B. Zhu, and Y. P. Sun, Exploring High-Performance p-Type Transparent Conducting Oxides Based on Electron Correlation in V_2O_3 Thin Films, Phys. Rev. Appl. **12**, 044035 (2019).

[5] *Handbook of Transparent Conductors* (Springer US, Boston, MA, 2011).

[6] X. Zhang, L. Zhang, J. D. Perkins, and A. Zunger, Intrinsic Transparent Conductors without Doping, Phys. Rev. Lett. **115**, 176602 (2015).

[7] O. I. Malyi, M. T. Yeung, K. R. Poeppelmeier, C. Persson, and A. Zunger, Spontaneous non-stoichiometry and ordering in degenerate but gapped transparent conductors, Matter **1**, 280 (2019).

[8] O. I. Malyi and A. Zunger, False metals, real insulators, and degenerate gapped metals, Appl. Phys. Rev. **7**, 041310 (2020).

[9] A. Zunger and O. I. Malyi, Understanding doping of quantum materials, Chem. Rev. **121**, 3031 (2021).

[10] E. Pavarini, S. Biermann, A. Poteryaev, A. I. Lichtenstein, A. Georges, and O. K. Andersen, Mott Transition and Suppression of Orbital Fluctuations in Orthorhombic $3d^1$ Perovskites, Phys. Rev. Lett. **92**, 176403 (2004).

[11] E. Pavarini, Solving the strong-correlation problem in materials, Riv. Nuovo Cimento **44**, 597 (2021).

[12] C.-N. Yeh, S. Iskakov, D. Zgid, and E. Gull, Electron correlations in the cubic paramagnetic perovskite Sr(V,Mn)O$_3$: Results from fully self-consistent self-energy embedding calculations, Phys. Rev. B **103**, 195149 (2021).

[13] L. Craco, M. S. Laad, S. Leoni, and E. Müller-Hartmann, Insulator-metal transition in the doped $3d^1$ transition metal oxide LaTiO$_3$, Phys. Rev. B **70**, 195116 (2004).

[14] A. Y. Ramos, C. Piamonteze, H. C. N. Tolentino, N. M. Souza-Neto, O. Bunau, Y. Joly, S. Grenier, J.-P. Itié, N. E. Massa, J. A. Alonso, and M. J. Martinez-Lope, Stability of Ni sites across the pressure-induced insulator-to-metal transition in YNiO$_3$, Phys. Rev. B **85**, 045102 (2012).

[15] E. Pavarini, A. Yamasaki, J. Nuss, and O. K. Andersen, How chemistry controls electron localization in $3d^1$ perovskites: A Wannier-function study, New J. Phys. **7**, 188 (2005).

[16] A. Glazer, The classification of tilted octahedra in perovskites, Acta Crystallogr., Sect. B: Struct. Crystallogr. Cryst. Chem. **28**, 3384 (1972).

[17] H. A. Jahn and E. Teller, Stability of polyatomic molecules in degenerate electronic states - I— orbital degeneracy, Proc. R. Soc. London, Ser. A **161**, 220 (1937).

[18] J. A. Alonso, J. L. Garcia-Munoz, M. T. Fernandez-Diaz, M. A. G. Aranda, M. J. Martinez-Lope, and M. T. Casais, Charge Disproportionation in RNiO$_3$ Perovskites: Simultaneous Metal-Insulator and Structural Transition in YNiO$_3$, Phys. Rev. Lett. **82**, 3871 (1999).

[19] M. Takano, N. Nakanishi, Y. Takeda, S. Naka, and T. Takada, Charge disproportionation in CaFeO$_3$ studied with the Mössbauer effect, Mater. Res. Bull. **12**, 923 (1977).

[20] J. Varignon, M. N. Grisolia, J. Íñiguez, A. Barthélémy, and M. Bibes, Complete phase diagram of rare-earth nickelates from first-principles, npj Quantum Mater. **2**, 21 (2017).

[21] J. Varignon, M. Bibes, and A. Zunger, Mott gapping in 3d ABO$_3$ perovskites without Mott-Hubbard interelectronic repulsion energy U, Phys. Rev. B **100**, 035119 (2019).

[22] J. Varignon, M. Bibes, and A. Zunger, Origin of band gaps in 3d perovskite oxides, Nat. Commun. **10**, 1658 (2019).

[23] O. I. Malyi, X.-G. Zhao, A. Bussmann-Holder, and A. Zunger, Local positional and spin symmetry breaking as a source of magnetism and insulation in paramagnetic EuTiO$_3$, Phys. Rev. Mater. **6**, 034604 (2022).

[24] H. Park, A. J. Millis, and C. A. Marianetti, Computing total energies in complex materials using charge self-consistent DFT + DMFT, Phys. Rev. B **90**, 235103 (2014).

[25] H. Park, A. J. Millis, and C. A. Marianetti, Total energy calculations using DFT + DMFT: Computing the pressure phase diagram of the rare earth nickelates, Phys. Rev. B **89**, 245133 (2014).

[26] A. B. Georgescu and A. J. Millis, Quantifying the role of the lattice in metal–insulator phase transitions, Commun. Phys. **5**, 135 (2022).

[27] A. Hampel, P. Liu, C. Franchini, and C. Ederer, Energetics of the coupled electronic–structural transition in the rare-earth nickelates, npj Quantum Mater., **4**, 5 (2019).

[28] A. Subedi, O. E. Peil, and A. Georges, Low-energy description of the metal-insulator transition in the rare-earth nickelates, Phys. Rev. B **91**, 075128 (2015).

[29] Z. Wang, O. I. Malyi, X. Zhao, and A. Zunger, Mass enhancement in 3d and s−p perovskites from symmetry breaking, Phys. Rev. B **103**, 165110 (2021).

[30] J. L. Du, O. I. Malyi, S. L. Shang, Y. Wang, X. G. Zhao, F. Liu, A. Zunger, and Z. K. Liu, Density functional thermodynamic description of spin, phonon and displacement degrees of freedom in antiferromagnetic-to-paramagnetic phase transition in YNiO$_3$, Mater. Today Phys. **27**, 100805 (2022).

[31] D. Gambino, O. I. Malyi, Z. Wang, B. Alling, and A. Zunger, Density functional description of spin, lattice, and spin-lattice dynamics in antiferromagnetic and paramagnetic phases at finite temperatures, Phys. Rev. B **106**, 134406 (2022).

[32] A. Mercy, J. Bieder, J. Iniguez, and P. Ghosez, Structurally triggered metal-insulator transition in rare-earth nickelates, Nat. Commun. **8**, 1677 (2017).

[33] G. Demazeau, A. Marbeuf, M. Pouchard, and P. Hagenmuller, Sur une série de composés oxygènes du nickel trivalent derivés de la perovskite, J. Solid State Chem. **3**, 582 (1971).

[34] H. Park, A. J. Millis, and C. A. Marianetti, Site-Selective Mott Transition in Rare-Earth-Element Nickelates, Phys. Rev. Lett. **109**, 156402 (2012).

[35] G. Trimarchi, Z. Wang, and A. Zunger, Polymorphous band structure model of gapping in the antiferromagnetic and paramagnetic phases of the Mott insulators MnO, FeO, CoO, and NiO, Phys. Rev. B **97**, 035107 (2018).

[36] I. Leonov, D. Korotin, N. Binggeli, V. I. Anisimov, and D. Vollhardt, Computation of correlation-induced atomic displacements and structural transformations in paramagnetic KCuF$_3$ and LaMnO$_3$, Phys. Rev. B **81**, 075109 (2010).

[37] X. Ren, I. Leonov, G. Keller, M. Kollar, I. Nekrasov, and D. Vollhardt, LDA-DMFT computation of the electronic spectrum of NiO, Phys. Rev. B **74**, 195114 (2006).

[38] G. Kresse and J. Hafner, Ab Initio Molecular Dynamics for Liquid Metals, Phys. Rev. B **47**, 558 (1993).

[39] G. Kresse and J. Furthmüller, Efficiency of ab-initio total energy calculations for metals and semiconductors using a plane-wave basis set, Comput. Mater. Sci. **6**, 15 (1996).

[40] G. Kresse and J. Furthmüller, Efficient iterative schemes for ab initio total-energy calculations using a plane-wave basis set, Phys. Rev. B **54**, 11169 (1996).

[41] J. P. Perdew, A. Ruzsinszky, G. I. Csonka, O. A. Vydrov, G. E. Scuseria, L. A. Constantin, X. Zhou, and K. Burke, Restoring the Density-Gradient Expansion for Exchange in Solids and Surfaces, Phys. Rev. Lett. **100**, 136406 (2008).

[42] S. L. Dudarev, G. A. Botton, S. Y. Savrasov, C. J. Humphreys, and A. P. Sutton, Electron-energy-loss spectra and the structural stability of nickel oxide: An LSDA + U study, Phys. Rev. B **57**, 1505 (1998).

[43] K. Momma and F. Izumi, VESTA 3 for three-dimensional visualization of crystal, volumetric and morphology data, J. Appl. Crystallogr. **44**, 1272 (2011).

[44] S. P. Ong, W. D. Richards, A. Jain, G. Hautier, M. Kocher, S. Cholia, D. Gunter, V. L. Chevrier, K. A. Persson, and G. Ceder, Python materials genomics (Pymatgen): A robust, open-source python library for materials analysis, Comput. Mater. Sci. **68**, 314 (2013).

[45] A. Zunger, S.-H. Wei, L. G. Ferreira, and J. E. Bernard, Special Quasirandom Structures, Phys. Rev. Lett. **65**, 353 (1990).